universe

MDPI

Article

A Catalog and Statistical Overview of TESS Eclipsing Binaries: Stellar and Orbital Parameters with Spectroscopic Constraints

Xinyu Wang [1,2,3], Yajuan Lei [1,2,3,*], Yanxia Zhang [1] and Guangwei Li [1]

[1] National Astronomical Observatories, Chinese Academy of Sciences, Beijing 100101, China; wxy@bao.ac.cn (X.W.); zyx@bao.ac.cn (Y.Z.); lgw@bao.ac.cn (G.L.)
[2] School of Astronomy and Space Science, University of Chinese Academy of Sciences, Beijing 100049, China
[3] State Key Laboratory of Solar Activity and Space Weather, Beijing 100190, China
* Correspondence: yjlei@bao.ac.cn

Abstract

Eclipsing binaries with spectroscopic constraints are fundamental benchmarks for stellar astrophysics, with detached double-lined systems providing dynamical masses and radii that are largely independent of stellar-evolution models. The Transiting Exoplanet Survey Satellite (*TESS*) has greatly expanded the photometric sample of eclipsing binaries, but systems with combined *TESS* light-curve and spectroscopic solutions remain dispersed across the literature. We present a literature catalog of 280 *TESS*-observed eclipsing binaries with published spectroscopic constraints compiled from 121 peer-reviewed studies through December 2025. The sample contains 228 double-lined and 52 single-lined spectroscopic binaries, of which 247 are not included in Eker et al. (2014). By analyzing the period–eccentricity distribution, we confirm previous studies showing that tidal circularization depends on stellar type: convective systems exhibit circularization at longer periods (Hot–Cold: $P_{\rm circ} \approx 6.2$ d; Cold–Cold: $P_{\rm circ} \approx 7.4$ d) compared to radiative systems ($P_{\rm circ} \approx 3.5$ d). We also constrain the maximum-eccentricity envelopes, which extend to longer periods in convective systems (Hot–Cold: $P_{\rm env} \approx 3.2$ d; Cold–Cold: $P_{\rm env} \approx 6.3$ d) than in radiative ones ($P_{\rm env} \approx 1.1$ d). We further define a main-sequence comparison sample of 345 components, 62 overlapping the detached-SB2 sample of Eker et al. (2018). Their mass–luminosity, mass–radius, and mass–effective-temperature distributions are consistent with the Eker et al. (2018) empirical relations. We also note a mild radius inflation for low-mass components ($M < 0.8 M_{\odot}$) compared to standard stellar evolution models , with a mean fractional radius inflation of $\sim 8.4\%$. The catalog provides a uniformly compiled stellar and orbital parameters; traceable, machine-readable resource for target selection; detached-SB2 benchmark construction; and follow-up studies of stellar parameters and binary interaction.

Keywords: eclipsing binaries; stellar fundamental parameters; catalogs; statistics

Check for updates

Academic Editor: Laszlo Szabados

Received: 29 September 2026
Revised: 13 November 2026
Accepted: 16 November 2026
Published: 20 November 2026

Copyright: © 2026 by the authors. Licensee MDPI, Basel, Switzerland. This article is an open access article distributed under the terms and conditions of the Creative Commons Attribution (CC BY) license.

1. Introduction

Binary and multiple systems are common outcomes of star formation and provide fundamental constraints on stellar structure and evolution. Among them, detached double-lined eclipsing binaries (SB2s) are particularly important because their orbital scales and component masses can be determined from the radial-velocity amplitudes and orbital inclination, while eclipse light curves constrain the inclination and fractional radii. The resulting masses and radii are therefore largely independent of stellar-evolution models. By contrast, effective temperatures and luminosities may retain systematic uncertainties associated with

atmosphere models, extinction corrections, flux calibration, and bolometric corrections. Detached SB2s thus serve as powerful empirical calibrators of mass–radius relations and stellar-evolution calculations, whereas semi-detached and contact binaries provide complementary laboratories for studying mass transfer, tidal effects, angular-momentum evolution, and binary interaction e.g., [1–4].

The benchmark value of eclipsing binaries has increased substantially with the advent of wide-field time-domain surveys. Launched in 2018, the Transiting Exoplanet Survey Satellite (*TESS*) [5] has provided high-precision, single-band photometry over a large fraction of the sky. Although *TESS* was designed primarily for exoplanet discovery, its light curves are also well suited to refining eclipse ephemerides, constraining eclipse geometry, detecting pulsations and spot modulation, and identifying systems that merit spectroscopic follow-up. Nevertheless, *TESS* photometry alone is usually insufficient for deriving complete physical solutions. A single *TESS* band constrains the temperature ratio more directly than two independent component temperatures, and accurate absolute temperatures commonly require spectroscopy, spectral-energy-distribution fitting, or multi-band photometry. Precise component masses and radii likewise require time-resolved spectroscopy in addition to photometric modeling. Consequently, the subset of *TESS*-observed eclipsing binaries with published spectroscopic constraints is much smaller than the full photometric candidate sample, and its orbital and stellar parameters remain dispersed across individual studies.

The importance of eclipsing binaries as empirical benchmarks has long been recognized, and several compilations have assembled high-quality parameters for such systems. Andersen [1] systematically compiled mass and radius data for 45 detached SB2s, with uncertainties below 2%. Torres et al. [2] expanded this sample to 94 systems, with uncertainties below 3%. Eker et al. [3] established a parameter set for 257 detached SB2 systems, corresponding to 514 stars, and reported mass and radius uncertainties better than 5% for 388 stars. Southworth [4] further updated the detached eclipsing-binary sample to 348 systems. More recently, Xiong et al. [6] compiled 184 detached systems, including 56 newly identified binaries from the LAMOST survey, while Rowan et al. [7] combined ASAS-SN and Gaia DR3 information to determine the masses and radii of 122 stars.

These catalogs provide valuable reference samples, but they were assembled for different scientific purposes and adopt different selection functions, quality criteria, and parameter conventions. The present work is designed as a *TESS* index of published eclipsing binaries with spectroscopic constraints. Its purpose is not to replace radial-velocity measurements or the detailed modeling performed in the original studies: any new joint orbital solution still requires the original radial velocities or newly acquired spectra. Rather, the catalog places published constraints, provenance information, uncertainties, parameter origins, and cautionary flags into a common searchable format, enabling target selection, follow-up planning, and reproducible construction of application-specific subsamples.

In this work, we compile published stellar and orbital parameters for *TESS* eclipsing binaries with spectroscopic constraints. The catalog includes detached, semi-detached, and contact systems, and it retains both SB2s and single-lined spectroscopic binaries (SB1s). This inclusive design preserves the breadth of the published *TESS* literature while allowing users to construct stricter subsamples for specific applications.

Eker et al. [8] established interrelated mass–luminosity, mass–radius, and mass–effective-temperature relations from 509 main-sequence stars in detached SB2 systems over $0.179\,M_{\odot} \leq M \leq 31\,M_{\odot}$. We use these relations as an external empirical reference for assessing the consistency of the compiled parameters. After separating components consistent with the main-sequence band from evolved, compact, and interacting systems, the selected comparison sample follows the expected Eker et al. relations within the scatter introduced by the heterogeneous source literature. This comparison provides an external

consistency check on the catalog compilation and helps identify the subset most appropriate for future stellar-model tests.

The structure of this paper is as follows. Section 2 describes the literature search, selection criteria, and sample definition. Section 3 presents the catalog construction, uniform compilation procedure, and recommended quality flags. Section 4 summarizes the statistical properties of the sample. Section 5 discusses representative applications and selection effects. Section 6 summarizes the main results.

2. Sample Definition and Literature Compilation

2.1. Literature Search and Selection Criteria

We searched the peer-reviewed literature for eclipsing-binary systems observed by *TESS* and having published spectroscopic constraints on the binary orbit. The compilation covers studies published between the launch of *TESS* in 2018 and December 2025. Candidate papers were identified through NASA ADS searches using keywords related to eclipsing binaries, followed by manual inspection of the relevant cited and citing literature. We retained only systems for which the adopted solution explicitly combined *TESS* photometry with published spectroscopic information.

A system was included in the catalog if it satisfied all of the following criteria:

1. The analysis was published in a peer-reviewed journal;
2. The system was identified as an eclipsing binary observed by *TESS*;
3. The published analysis used time-resolved spectroscopy or reported radial-velocity constraints tied to the binary orbit;
4. At least one radial-velocity semi-amplitude or a spectroscopic orbital solution was provided;
5. The paper reported component parameters or sufficient orbital and stellar information to record or infer at least part of the stellar-parameter set.

Systems with only photometric binary solutions were excluded. Candidate eclipsing binaries without published spectroscopic constraints were also excluded, even when their *TESS* light curves showed well-defined eclipses. The resulting catalog is therefore a literature-based compilation of spectroscopically constrained *TESS* eclipsing binaries, not a complete inventory of all *TESS* eclipsing binaries or a statistically complete survey sample.

2.2. Treatment of Multiple Literature Solutions

Some binaries have been analyzed in more than one publication. When multiple solutions were available, we adopted the solution that provided the most complete, internally consistent, and well-documented set of orbital and stellar parameters. Preference was given to studies that combined *TESS* light-curve modeling with radial-velocity constraints, reported uncertainties for the principal fitted or derived quantities, and clearly described the underlying modeling assumptions. When a system was classified as SB1 in one study but was later resolved as SB2 using comparable or improved spectroscopic data, we adopted the SB2 solution. When a single paper presented multiple models, we adopted the model identified by the original authors as their preferred solution. Cases requiring additional judgment, including inconsistent parameter definitions, ambiguous component labels, or non-standard modeling assumptions, were retained with notes in the catalog.

The final compilation contains 280 eclipsing-binary systems drawn from 121 peer-reviewed publications. The sample includes 228 SB2 systems and 52 SB1 systems. By binary morphology, the catalog contains 249 detached, 19 semi-detached, and 12 contact binaries.

2.3. Caveat on SB1 Systems

For SB2 eclipsing binaries, the combination of light-curve modeling and radial-velocity curves can determine the orbital scale and yield dynamical masses and radii for both components. The inclination and fractional radii are constrained by the eclipses, while the radial-velocity amplitudes set the absolute scale of the orbit. In contrast, for SB1 systems, only the radial velocity of the visible component is measured directly. The mass of the unseen companion is constrained through the mass function and generally requires additional assumptions or external information, such as an adopted primary mass, inclination constraint, spectral-energy-distribution modeling, or evolutionary priors. Accordingly, SB1 companion parameters are treated in this catalog as inferred or model-dependent quantities, and the SB1/SB2 classification is explicitly flagged. This distinction is essential when constructing detached-SB2 benchmark samples for stellar-model tests, for which directly constrained dynamical masses and radii are preferred.

3. Catalog Construction and Uniform Compilation

3.1. Catalog Contents

The catalog is a literature-based compilation. We do not re-fit or homogenize the published solutions; instead, we convert the literature values to uniform units, adopt consistent definitions for derived quantities, propagate uncertainties where possible, and record provenance and quality flags. The catalog contains one row per binary system. The main columns include the *TESS* Input Catalog (TIC) identifier, alternative name, equatorial coordinates, *TESS* magnitude, orbital period, binary morphology, semi-major axis, inclination, eccentricity, systemic velocity, radial-velocity semi-amplitudes, mass ratio, component effective temperatures, component masses, component radii, surface gravities, luminosities, parameter uncertainties, solution code, literature reference, and notes. The machine-readable table also includes quality flags for compact, interacting, grazing, ambiguous, or otherwise model-dependent cases.

A shortened version of the column dictionary is shown in Table 1. Tables 2–4 present five systems chosen to illustrate the types of missing values in the catalog. These include missing eccentricity or temperature uncertainties (TIC 54957535, TIC 149319411); missing secondary temperatures and masses (TIC 234211934, TIC 57258016); absent semi-major axis, inclination, and velocity amplitudes (TIC 57258016, TIC 157376469, TIC 149319411); and missing systemic velocities and luminosities (TIC 157376469, TIC 149319411, TIC 234211934). Dashes indicate where such information is unavailable in the source publication. The complete catalog, including all orbital, stellar, uncertainty, provenance, reference, and note columns, is provided in machine-readable form (see Table S1 in the Supplementary Materials).

3.2. Uniform Compilation and Parameter Conventions

The literature values were converted to uniform units. Periods are reported in days, radial velocities in km s^{-1}, masses in $M_\odot$, radii and semi-major axes in $R_\odot$, effective temperatures in K, and surface gravities in cgs units. For parameters with asymmetric uncertainties, we adopt the larger of the upper and lower uncertainties as a conservative single error bar. Blank entries indicate that a quantity was not available in the adopted source or could not be reliably inferred from the published information. Upper limits, lower limits, and quantities requiring special treatment are retained but flagged separately from standard measurements.

The mass ratio is defined as

$$q = \frac{M_2}{M_1}, \tag{1}$$

where the component labels follow the convention of the adopted reference. We do not relabel the components to impose a universal ordering by mass, temperature, luminosity,

or eclipse depth. This choice preserves traceability to the original literature, but it also means that M_1 and M_2 should be interpreted as literature-defined components rather than as uniformly compiled primary and secondary stars. In many detached SB2 systems, the primary is also the hotter, brighter, or more massive component, but this convention is not universal, especially for evolved, interacting, contact, or mass-transfer systems. Users should therefore consult the original reference, notes, and flags when interpreting systems with $q > 1$, evolved components, or ambiguous primary/secondary designations. For SB1 systems, the definition of q likewise follows the adopted reference, and companion parameters should be treated as inferred or model-dependent quantities.

Table 1. Representative catalog columns.

Column	Unit	Description
TIC number	...	TIC identifier
Other Name	...	Common name or alternative identifier
RAJ2000	deg	Right ascension in J2000
DECJ2000	deg	Declination in J2000
TESS magnitude	mag	*TESS*-band magnitude
Orbital Period	day	Orbital period
Type	...	SB1 or SB2 classification
Class	...	Detached, semi-detached, or contact
a	$R_\odot$	Orbital semi-major axis $(a_1 + a_2)$
i	deg	Orbital inclination
e	...	Orbital eccentricity
e_{fixed}	...	Y, N or upper-limit
q	...	Mass ratio, defined as M_2/M_1
T_1, T_2	K	Component effective temperatures
M_1, M_2	$M_\odot$	Component masses
R_1, R_2	$R_\odot$	Component radii
$\log g_1$, $\log g_2$	dex	Component surface gravities
$\log L_1$, $\log L_2$	dex	Component luminosities in $\log(L/L_\odot)$
K_1, K_2	km s^{-1}	Radial-velocity semi-amplitudes
V_γ	km s^{-1}	Systemic radial velocity
Code	...	The code used in each adopted solution
Reference	...	Literature reference

The complete table is provided in machine-readable form (Table S1 in the Supplementary Materials). A portion is shown here for guidance regarding its form and content.

Table 2. Identifiers and orbital parameters of five selected systems containing missing entries in the catalog.

TIC Number	Other Name	R.A. (deg)	Decl. (deg)	T_{mag} (mag)	P_{orb} (day)	a ($R_\odot$)	i (deg)	e
TIC 157376469	V* V1361 Her	238.7754024	42.90045442	13.869	1.34117 ± 0.000006	5.501 ± 0.074	87.589 ± 0.055	0.0017 ± 0.0002
TIC 234211934	2MASS J06464003+0109157	101.6668012	1.154376873	11.442	1.06493559 ± 0.00000075	2.72 ± 0.05	83.6 ± 0.3	0.016 ± 0.007
TIC 54957535	TYC 5450-1192-1	130.985253	−11.55765757	10.246	0.7928396 ± 0.0000002	4.32 ± 0.03	73.6 ± 0.1	0.0000
TIC 149319411	TYC 7110-2486-1	115.9493329	−32.12252602	9.495	4.752212 ± 0.000008	22.041 ± 0.001	83.6027 ± 0.0008	0.0042 ± 0.0004
TIC 57258016	V* V916 Her	251.6478742	41.79228833	7.662	19.69846 ± 0.00001	…	…	0.57 ± 0.01

… indicates entries that are missing or not available in the source catalog; data without an uncertainty are quoted as such because the original literature did not provide a published error.

Table 3. Stellar parameters of five selected systems.

TIC Number	T_1 (K)	T_2 (K)	M_1 ($M_\odot$)	M_2 ($M_\odot$)	R_1 ($R_\odot$)	R_2 ($R_\odot$)	$\log g_1$ (dex)	$\log g_2$ (dex)
TIC 157376469	4740 ± 45	4169 ± 100	0.704 ± 0.028	0.539 ± 0.021	0.754 ± 0.01	0.543 ± 0.007	4.53 ± 0.22	4.7 ± 0.23
TIC 234211934	3870 ± 26	…	0.571 ± 0.017	0.565 ± 0.013	0.659 ± 0.053	0.57 ± 0.06	4.56 ± 0.71	4.72 ± 0.74
TIC 54957535	6960 ± 120	9870 ± 310	1.733 ± 0.031	0.22 ± 0.008	2.094 ± 0.013	0.331 ± 0.003	4.035 ± 0.003	4.741 ± 0.013
TIC 149319411	12500	11731	3.16 ± 0.01	3.2 ± 0.01	2.307 ± 0.002	2.377 ± 0.003	4.212 ± 0.002	4.191 ± 0.002
TIC 57258016	7000 ± 300	7250 ± 300	…	…	2.5 ± 0.2	2.3 ± 0.2	3.5	3.5

Table 4. Luminosities and spectroscopic parameters of five selected systems.

TIC Number	$\log(L_1/L_\odot)$	$\log(L_2/L_\odot)$	K_1 (km s^{-1})	K_2 (km s^{-1})	V_γ (km s^{-1})	Code	ADS Bibcode	Notes
TIC 157376469	−0.5883 ± 0.0354	−1.0969 ± 0.0326	…	…	…	WD	2021PASP..133d4202P	…
TIC 234211934	…	…	107.6 ± 0.7	108.6 ± 1.4	67.13 ± 0.52	ellc	2021PASP..133d4201M	The paper adopts the APOGEE value of 3870 K as an approximation for the primary's effective temperature.
TIC 54957535	0.968 ± 0.03	−0.028 ± 0.055	31.1 ± 0.9	244.7 ± 1.5	54.2 ± 0.1	WD	2021AJ....161..137H	The secondary is a pre-He WD.
TIC 149319411	2.066	1.982	…	…	…	PHOEBE	2019MNRAS.490.4154S	T_2 is derived from the literature T_2/T_1 ratio.
TIC 57258016	1.127 ± 0.075	1.124 ± 0.075	71.4 ± 0.2	72.3 ± 0.2	−14.26 ± 0.05	RV orbit + spectroscopy + photometry	2024A&A...685A.133C	No secondary eclipse; the grazing geometry; radii and logg are derived from spectral synthesis.

3.3. General Methodology for Orbital Solutions and Derived Parameters

This section summarizes the general framework used in the literature to derive stellar masses and radii from joint modeling of photometric light curves and spectroscopic radial velocities. For a spectroscopic binary, the radial velocity of component i can be written as

$$RV_i = \gamma + K_i[\cos(\nu + \omega) + e\cos\omega], \tag{2}$$

where γ is the systemic velocity, K_i is the radial-velocity semi-amplitude, ν is the true anomaly, ω is the argument of periastron, and e is the eccentricity. The semi-amplitude is related to the projected semi-major axis by

$$K_i = \frac{2\pi a_i \sin i}{P\sqrt{1-e^2}}, \tag{3}$$

or equivalently,

$$a_i \sin i = \frac{K_i P\sqrt{1-e^2}}{2\pi}. \tag{4}$$

For an SB2 eclipsing binary, the component masses are given by

$$M_1 \sin^3 i = \frac{P(1-e^2)^{3/2}}{2\pi G}(K_1 + K_2)^2 K_2, \tag{5}$$

and

$$M_2 \sin^3 i = \frac{P(1-e^2)^{3/2}}{2\pi G}(K_1 + K_2)^2 K_1. \tag{6}$$

The light-curve solution constrains the orbital inclination and fractional radii, thereby allowing the absolute orbital scale and component radii to be determined. For SB1 systems, the spectroscopic orbit instead yields the mass function,

$$f(M) = \frac{M_2^3 \sin^3 i}{(M_1 + M_2)^2} = \frac{PK_1^3(1-e^2)^{3/2}}{2\pi G}, \tag{7}$$

which constrains the companion mass but does not provide a unique model-independent solution without additional assumptions or external information.

The TESS light curves compiled in this catalog are not derived from a single, homogeneous processing pipeline; they are taken from the literature. It is therefore appropriate to briefly discuss the differences in data extraction and analysis so that readers can assess the consistency and reliability of the sample.

Regarding light-curve products, most studies use TESS Science Processing Operations Center (SPOC) data, either Simple Aperture Photometry (SAP) or Pre-search Data Conditioning SAP (PDCSAP); some use the MIT Quick Look Pipeline (QLP), and others perform custom aperture photometry directly on Full Frame Images (FFIs). These products differ in background subtraction, systematics correction, and treatment of long-term trends: PDCSAP has part of the low-frequency variability removed, SAP retains more of the original systematics, and custom FFI photometry depends on the choice of aperture and background mask. For detrending, common approaches include polynomial or spline fits, Gaussian process regression, wOTAN/Tukey biweight filtering, and linear regression against external parameters. These methods preserve out-of-eclipse modulation (spots, ellipsoidal variation, reflection) to different degrees, which can affect the fitted eclipse depth, radius ratio, and inclination, particularly for grazing or low-amplitude systems.

In the source literature, eclipsing-binary solutions are commonly obtained with the Wilson–Devinney (WD) code [9,10] or with PHOEBE [11,12], which model light curves and radial-velocity curves within a binary-geometry framework. Other codes such as JKTEBOP [13,14], ellc [15], LCURVE [16], and eb/EBOP [17] are also widely used. These

differ in their treatment of stellar shapes, limb-darkening laws, reflection, gravity darkening, and whether RV data are fitted simultaneously. Component effective temperatures are usually constrained using spectroscopy, spectral disentangling, spectral-energy-distribution fitting, multi-band photometry, or a combination of these methods. For spectroscopy and RVs, the literature commonly uses cross-correlation functions (CCF), least-squares deconvolution (LSD), spectral synthesis (e.g., ATLAS9/SYNTHE, ZEEMAN, iSpec), and SED fitting. In single-band TESS analyses, the light curve generally constrains the temperature ratio more directly than the absolute temperatures of both components; absolute temperature scales therefore often depend on spectroscopic or external photometric information.

These methodological differences—spanning data extraction, detrending, modeling codes, and temperature calibration—are one source of heterogeneity in the compiled literature parameters. When compiling them, we prioritized systems with explicit data-processing descriptions and self-consistent light-curve and RV solutions, and we indicate modeling code in the catalog so that readers can assess the consistency of the results.

When a quantity was not explicitly reported in the adopted source but could be derived from published parameters, we computed it uniformly. If both component masses were available, the mass ratio was calculated as $q = M_2/M_1$ under the component convention of the adopted reference. If component masses and radii were available, surface gravity was calculated as

$$\log g_i = \log g_\odot + \log\left(\frac{M_i}{M_\odot}\right) - 2\log\left(\frac{R_i}{R_\odot}\right), \tag{8}$$

where $\log g_\odot = 4.438$ was adopted. If effective temperature and radius were available, luminosity was calculated as

$$\log\left(\frac{L_i}{L_\odot}\right) = 2\log\left(\frac{R_i}{R_\odot}\right) + 4\log\left(\frac{T_i}{T_\odot}\right), \tag{9}$$

with $T_\odot = 5772$ K. Uncertainties were propagated using standard error propagation when the required input uncertainties were available.

4. Statistical Properties of the Catalog

4.1. Sample Composition

The catalog contains 280 *TESS* eclipsing binaries with published spectroscopic constraints, including 228 SB2 systems and 52 SB1 systems. Detached binaries dominate the sample, with 249 systems, while 19 systems are semi-detached, and 12 are contact binaries. This composition reflects both the suitability of detached eclipsing binaries for precise parameter determination and the observational selection of spectroscopic follow-up toward brighter, shorter-period, or otherwise well-characterized systems.

The catalog should not be interpreted as a volume-limited, magnitude-limited, or population-complete sample. It is a literature-based compilation of systems for which detailed modeling has already been published. Statistical trends derived from the catalog therefore describe the current spectroscopically characterized *TESS* eclipsing-binary literature, rather than the intrinsic distributions of the underlying *TESS* eclipsing-binary population.

4.2. Magnitude, Mass-Ratio, Period, and Eccentricity Distributions

Figure 1 and Table 5 summarize the distributions of *TESS* magnitude, orbital period, mass ratio, and eccentricity. The *TESS* magnitudes span 3.687–16.594 mag, with most systems concentrated between 7 and 12 mag and a peak in the 9–10 mag bin. The mass ratio, defined as $q = M_2/M_1$ under the component convention of the adopted reference, ranges from 0.07 to 2.335. Because component labels are inherited from the source literature, this distribution should be interpreted as a literature-defined mass-ratio distribution rather

than a uniformly compiled distribution of less-massive to more-massive components. The catalog contains 35 systems with $q > 1.0$; 33 of them have $1.0 < q < 1.25$, while the two systems with $q > 2.0$ are both contact binaries.

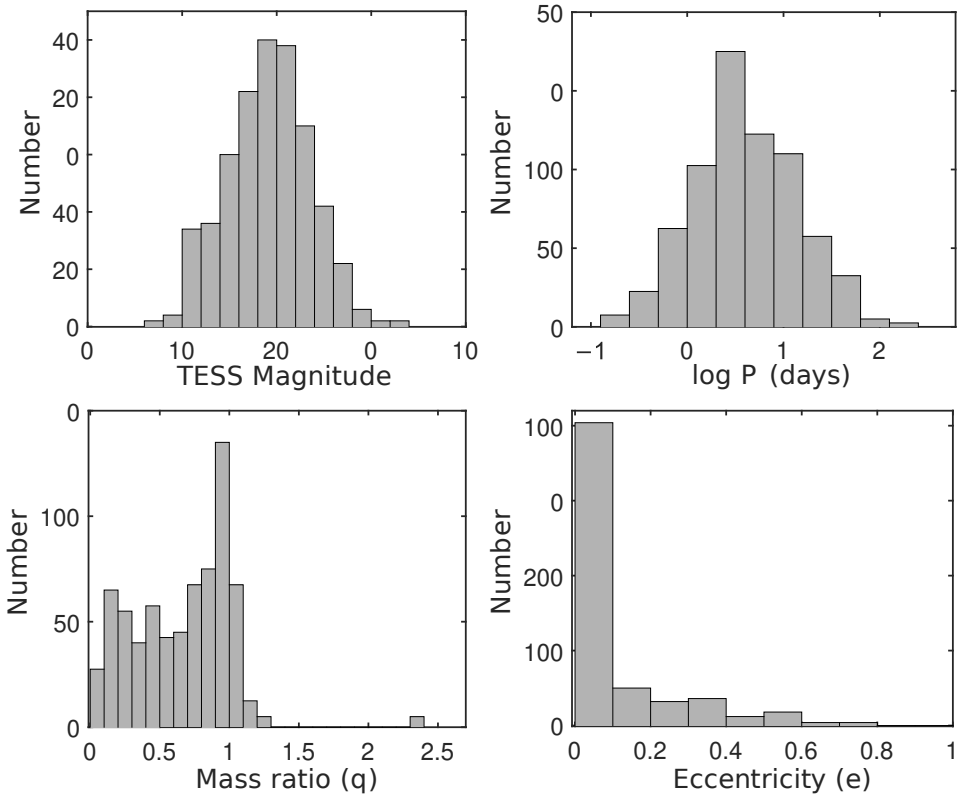

Figure 1. From top left to bottom right: TESS magnitude, orbital period, mass ratio ($q = M_2/M_1$) and orbital eccentricity. The sample is dominated by short-period, low-eccentricity systems.

Table 5. Summary statistics of system parameters in the sample.

	T_{mag}	P_{orb} (days)	e
Minimum	3.687	0.127037	0.0000
Maximum	16.594	193.35875	0.7821
Mean	9.560	8.634857	0.0940
Median	9.625	3.782342	0.0051

The period distribution is strongly weighted toward short-period systems: approximately 77% of the binaries have $P_{orb} < 10$ days, with a concentration at a few days. NGTS-EB-7 (TIC 238060327) is the only system with $P_{orb} > 70$ days and has the longest period in the catalog, $P_{orb} = 193.4$ days. The shortest-period system is TIC 242402846, a hot-subdwarf B plus M-dwarf binary with $P_{orb} = 0.127037$ days [18]. This short-period dominance reflects both the higher geometric eclipse probability of compact systems and the observational efficiency of obtaining multiple eclipses and adequate radial-velocity phase coverage.

The eccentricity distribution is similarly concentrated toward low values: approximately 72% of the systems have $e < 0.1$. This is consistent with the large fraction of short-period binaries, for which tidal dissipation tends to circularize the orbit, but it should also be interpreted in light of the selection effects of the literature sample. Long-period or high-eccentricity systems are relatively rare in the catalog, but they remain valuable targets for testing tidal evolution and binary-formation scenarios.

4.3. Effective Temperatures, Masses, and Radii

The component effective temperatures, masses, and radii span a broad range of stellar types (Figure 2). The effective temperatures of the primary stars span more than an order of magnitude, from 2930 K to 42,000 K. The hottest primaries are found in the massive detached binary WR 21a, which also hosts the highest secondary temperature in the sample, reaching 48,000 K. Most systems, however, have primary temperatures concentrated between 4000 K and 10,000 K, consistent with late-K to A-type stars, with a strong concentration among low- and intermediate-mass components.

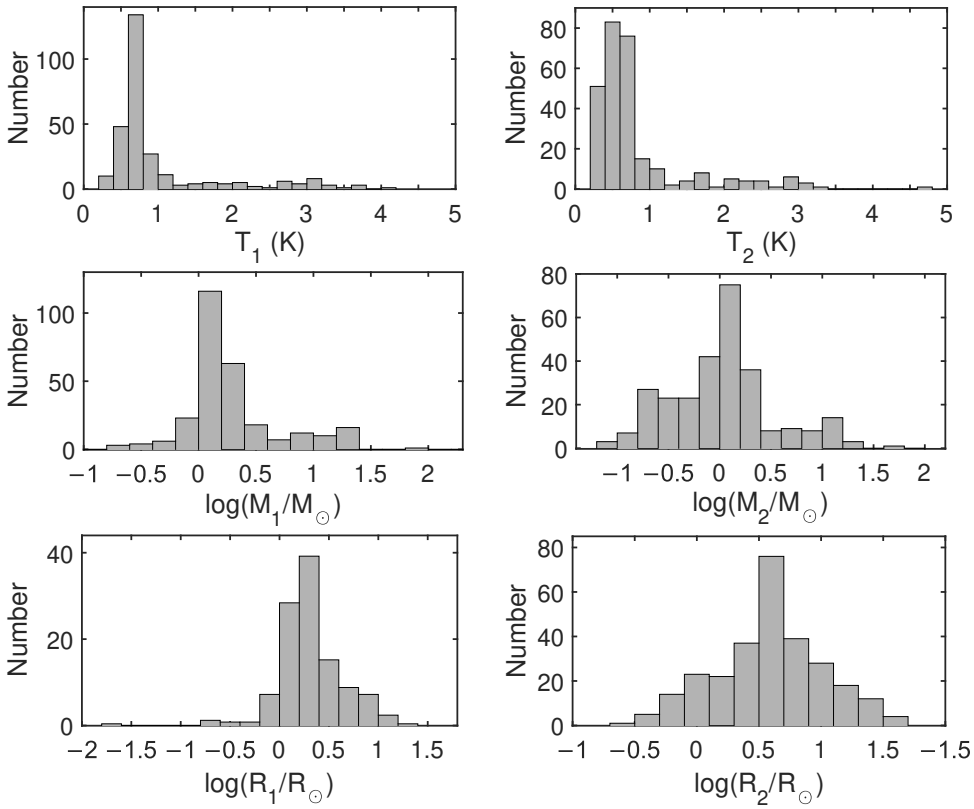

Figure 2. Distributions of component effective temperatures (**top**), masses (**middle**), and radii (**bottom**) for the compiled sample. Primary and secondary components are shown separately from original literatures.

Most components are low- to intermediate-mass stars, with approximately 87% having $M < 5\,M_{\odot}$ and approximately 90% having $R < 5\,R_{\odot}$. The catalog also includes a smaller number of compact, stripped, evolved, and massive systems, including white-dwarf and hot-subdwarf binaries. These systems are astrophysically valuable, but they should be treated separately when constructing statistical samples of ordinary main-sequence binaries.

Table 6 summarizes the fractional uncertainties of the four fundamental parameters, M_1, M_2, R_1, and R_2, in the compiled sample. For each parameter, we list the total number of systems with available measurements, the number of systems without reported uncertainties, and the cumulative counts of systems with relative uncertainties below 5%, 10%, and 20%. Most reported measurements have formal fractional uncertainties below 20%, including more than 95% of the mass measurements and more than 98% of the radius measurements. These statistics indicate that many literature-reported parameters are formally precise, but their physical interpretation depends on spectroscopic type, binary morphology, parameter provenance, and quality flags.

Table 6. Summary of reported formal uncertainties.

Parameter	N_{total}	$N_{\text{no error}}$	<5%	<10%	<20%
M_1	279	3	203	251	272
M_2	279	3	205	245	267
R_1	280	3	246	270	277
R_2	279	4	228	259	270

Overall, the catalog provides broad coverage in component mass and radius, from low-mass stars to massive, compact, and evolved objects. This coverage is useful for target selection and for identifying systems that would benefit from homogeneous photometric and spectroscopic reanalysis.

4.4. Notable Systems and Special Cases

Among the 280 systems in the catalog, 42 systems (15%; 25 SB2s and 17 SB1s) are assigned non-null quality flags to identify parameters or configurations that require additional caution. These flags fall into several broad categories. First, 12 systems contain compact or stripped components, including nine pre-He white dwarfs, one white dwarf, one sdB star, and one sdOB star. Second, 11 systems have absent, grazing, shallow, or otherwise unusual secondary eclipses, which can lead to weakly constrained or model-dependent secondary radii and effective temperatures; in some cases, only limits are available. Third, several entries involve eccentricity upper limits, which are parameters adopted from approximate radial-velocity quantities inferred from incomplete published information. Additional flags identify inconsistencies between published surface gravities and values recalculated from the reported masses and radii, component-swapped $\log g$ or luminosity values in the source literature, rapid rotation or tidal distortion, pulsations, unresolved higher-order multiplicity, and cases in which spectroscopic and model-derived mass ratios differ substantially.

These flags are not intended to label the affected measurements as erroneous. Rather, they record non-standard, model-dependent, or potentially ambiguous cases that users should inspect individually. They are especially important when constructing high-precision benchmark samples, for which compact objects, interacting systems, weakly constrained secondary parameters, or externally imposed stellar parameters may need to be excluded.

5. Discussion

Existing compilations such as Eker et al. [3], Southworth [4], and Xiong et al. [6] have primarily focused on high-precision detached eclipsing binaries or on selected benchmark samples. The present catalog has a different emphasis: it is organized around *TESS*-observed systems with TIC identifiers, *TESS* magnitudes, and published spectroscopic constraints, and it retains detached, semi-detached, and contact binaries as well as both SB2 and SB1 systems. The catalog shares 33 systems with Eker et al. [3], 22 with Southworth/DEBCat, and 25 with Xiong et al. [6], illustrating its complementarity to earlier detached-binary compilations.

This broader selection supports two main use cases. Detached SB2 systems with well-reported uncertainties and no interaction or quality flags can be selected for stellar-model comparisons and benchmark-sample construction. Semi-detached and contact systems, although unsuitable for calibrating single-star relations, are retained as useful targets for studies of mass transfer, tidal evolution, and binary interaction. The provenance and quality flags are intended to make these selections transparent and reproducible.

5.1. Period–Eccentricity Distribution

Figure 3 presents the period–eccentricity distribution for the compiled sample and the sample of Eker et al. [3]. The dominance of short-period, low-eccentricity systems reflects

both tidal circularization and observational selection. Most systems with orbital periods shorter than 10 days have eccentricities below 0.1, whereas longer-period systems span a wider eccentricity range, including highly eccentric systems such as NGTS-EB-7. These systems are useful targets for studies of tidal evolution and binary formation.

To study the relationship between orbital period and eccentricity across different stellar types, we divide the sample into three distinct groups: Hot–Hot, Hot–Cold, and Cold–Cold, adopting $T_{\rm eff} = 6250$ K as the boundary between hot stars with radiative envelopes and cool stars with convective envelopes, following the temperature thresholds established by Van Eylen et al. [19] and Justesen & Albrecht [20]. We perform independent nonlinear least-squares fits for each subsample using the functional form of Zanazzi [21]:

$$e = \alpha\left[1 - \left(\frac{P_{\rm circ}}{P}\right)^{\beta}\right], \tag{10}$$

where $P_{\rm circ}$ is the critical circularization period for nearly circular binaries, α is the asymptotic eccentricity plateau, and β governs the steepness. We also fit the eccentricity envelope period $P_{\rm env}$ following Zanazzi [21], which represents the shortest period out to which the most eccentric binaries are circularized. Parameter uncertainties are estimated via residual bootstrap resampling.

For the **Hot–Hot (radiative) binaries** (Figure 3, top), we obtain a short circularization period of $P_{\rm circ} = 3.5 \pm 0.8$ d ($\alpha = 0.36 \pm 0.06$, $\beta = 0.90 \pm 0.15$) and an empirical envelope of $P_{\rm env} = 1.1 \pm 0.2$ d ($\alpha = 0.51 \pm 0.03$). For the **Hot–Cold systems** (Figure 3, middle), circularization occurs at a significantly longer period, yielding $P_{\rm circ} = 6.2 \pm 0.6$ d ($\alpha = 0.36 \pm 0.08$, $\beta = 2.14 \pm 0.58$), with a notably steeper slope. The upper envelope yields $P_{\rm env} = 3.2 \pm 0.9$ d with $\alpha = 0.56 \pm 0.11$. For the **Cold–Cold systems** (Figure 3, bottom), we derive $P_{\rm circ} = 7.4 \pm 1.3$ d ($\alpha = 0.35 \pm 0.09$, $\beta = 1.00 \pm 0.33$) and an envelope period of $P_{\rm env} = 6.3 \pm 0.8$ d ($\alpha = 0.63 \pm 0.08$). The fitted $P_{\rm circ}$ values for the Hot–Cold and Cold–Cold groups are consistent (6.2 ± 0.6 d and 7.4 ± 1.3 d, respectively), and both are significantly longer than that of the Hot–Hot group (3.5 ± 0.8 d). This confirms that in mixed systems, tidal dissipation is primarily dictated by the cooler component's convective envelope, which overwhelms the contribution from the radiative hot component [19,20].

While the envelope period $P_{\rm env}$ of the Cold–Cold group (6.3 ± 0.8 d) is longer than that of the Hot–Cold group (3.2 ± 0.9 d), the discrepancy could be due to statistical limitations. As demonstrated by Zanazzi [21], $P_{\rm env}$ is sensitive to sample size; smaller samples tend to suffer from larger uncertainties. Nevertheless, the derived $P_{\rm circ}$ for both convective groups align with the 'two circularization periods' phenomenon reported by Zanazzi [21], suggesting a 'cold core' of long-period circular binaries alongside a population of short-period eccentric systems.

Conversely, the relatively short $P_{\rm circ}$ and $P_{\rm env}$ for the Hot–Hot sample reflect the weaker tidal dissipation in radiative envelopes, consistent with the standard dynamical-tide picture [20]. As found by Van Eylen et al. [19], Hot–Hot binaries are the group most likely to remain significantly eccentric at short periods ($P < 4$ d).

A subset of the literature solutions in our sample fixed the eccentricity at $e = 0$. This includes systems for which the adopted solution explicitly fixed the eccentricity to zero, as well as systems for which no eccentricity was reported and a circular orbit was implicitly assumed. Treating such fixed or assumed values as measurements could bias the derived circularization period. We therefore flagged all such systems and repeated the fit excluding them. The circularization periods and envelope parameters obtained with and without these systems agree within the uncertainties, indicating that solutions with fixed or assumed $e = 0$ do not significantly affect our conclusions. The flagged systems are also identified in the machine-readable catalog.

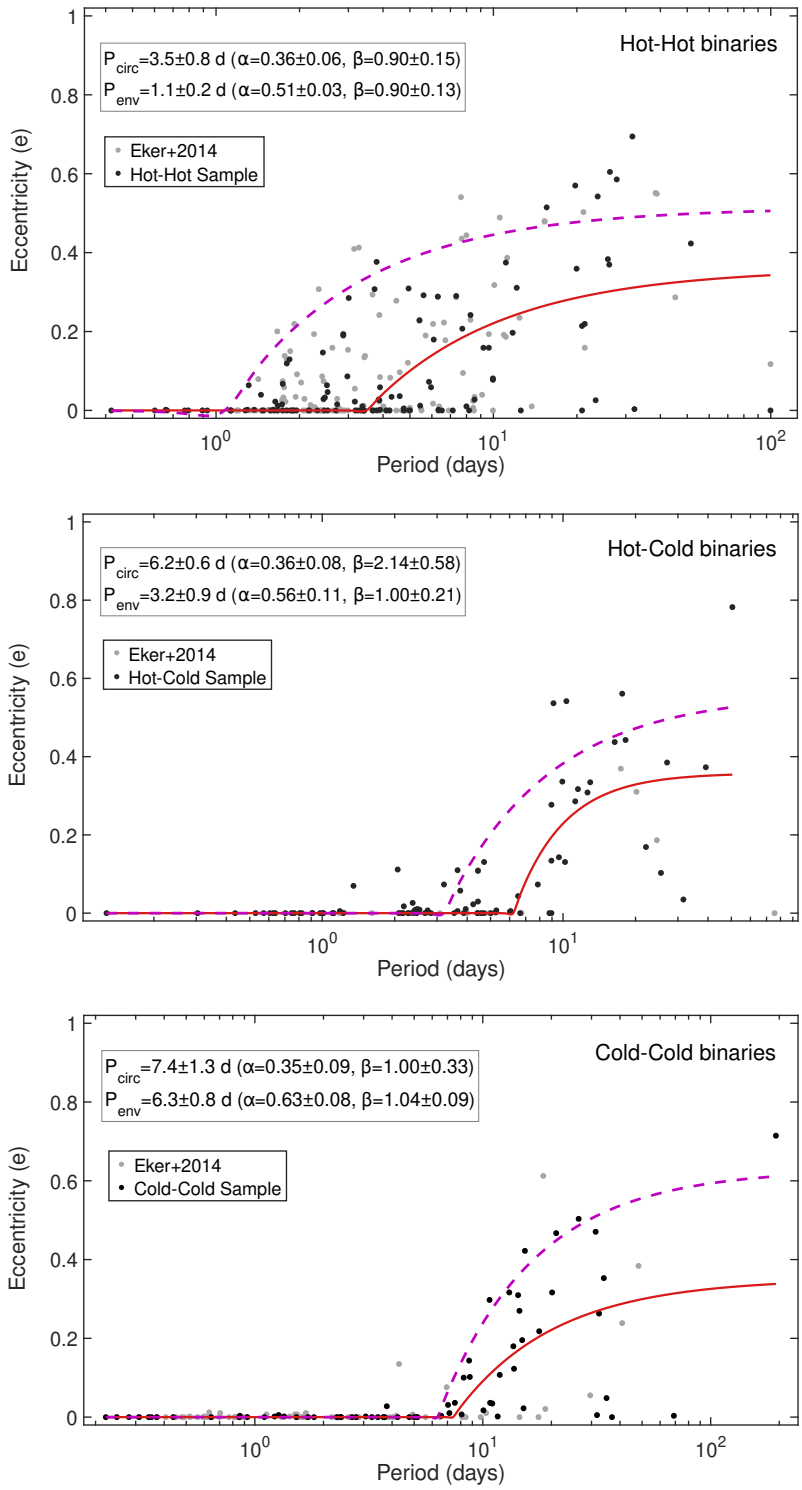

Figure 3. Period–eccentricity distribution for Hot–Hot binaries (**top panel**), Hot–Cold systems (**middle panel**), and Cold–Cold systems (**bottom panel**). The solid red curve is the best-fit Zanazzi [21] circularization model, and the magenta dashed curve is the empirical upper envelope. The gray points denote the Eker et al. [3] sample. The best-fit parameters ($P_{\rm circ}$, $P_{\rm env}$, α, β) and their uncertainties are displayed in the top-left legend of each panel.

5.2. Hertzsprung–Russell Diagram

Figure 4 shows the distribution of catalog components in the effective-temperature–luminosity plane. SB2 and SB1 systems are shown in the upper and lower panels, respectively, with symbols distinguishing detached, semi-detached, and contact binaries. The

dashed curves mark the theoretical Zero-Age Main Sequence (ZAMS; $Z = 0.008$) and Terminal-Age Main Sequence (TAMS; $Z = 0.040$) loci from the Padova and Trieste Stellar Evolution Code (PARSEC) models adopted by Eker et al. [8]. Most components lie on or near the main-sequence band, consistent with the dominance of detached systems with component masses below several solar masses. The hottest and most luminous objects correspond to massive systems such as WR 21a, whereas compact objects, including white dwarfs and hot subdwarfs, fall well below the main sequence.

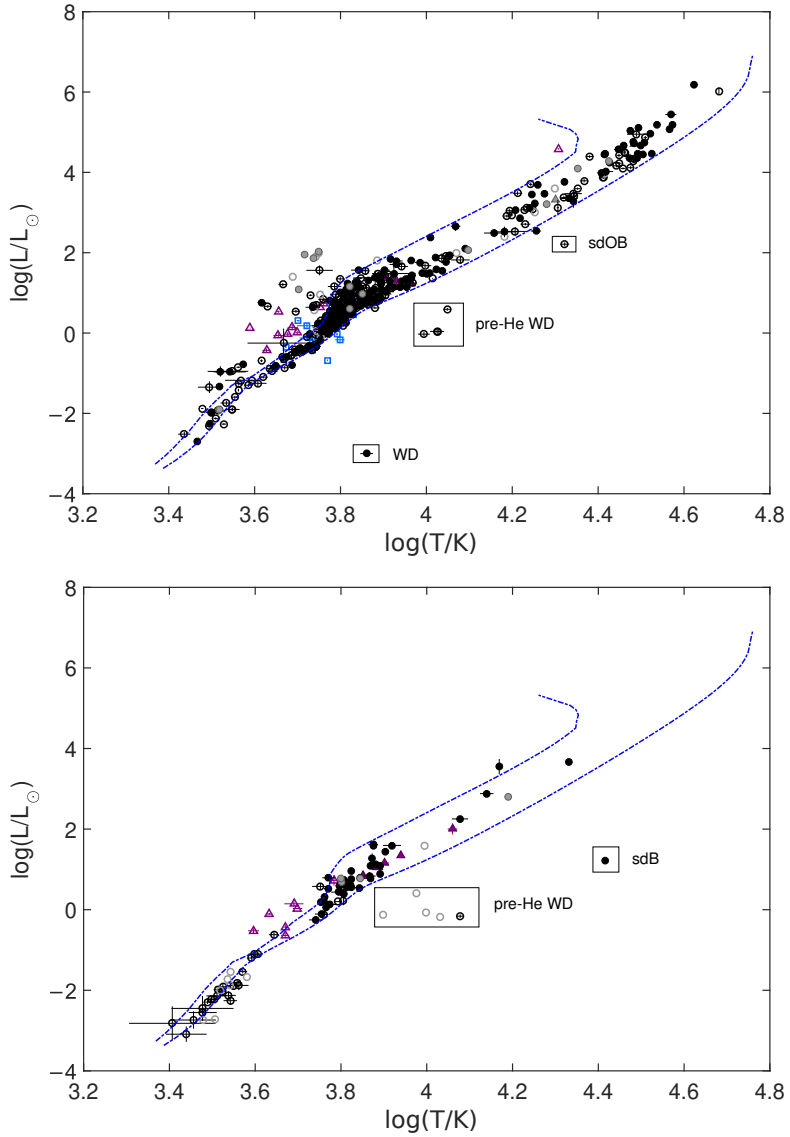

Figure 4. Hertzsprung–Russell diagram for catalog components. (**Upper panel**): SB2 sample; (**lower panel**): SB1 sample. Primary and secondary stars are shown with filled and open symbols, respectively. Gray symbols denote systems with no reported uncertainties; black symbols, purple triangles, and blue squares represent detached, semi-detached, and contact binaries, respectively. The dashed curves show the ZAMS and TAMS boundaries adopted from PARSEC models [22]. Several sources located below the ZAMS are labeled individually.

Semi-detached and contact binaries are expected to deviate more strongly from single-star evolutionary sequences because mass transfer, tidal distortion, and common-envelope evolution can alter their radii, temperatures, and luminosities relative to isolated stars of the same mass. These systems should therefore be treated separately when constructing

samples for single-star evolutionary tests, although they remain valuable laboratories for binary interaction.

The HR diagram provides a consistency check on the compiled parameters and a practical guide for selecting appropriate subsamples. It should not be interpreted as a complete representation of the underlying *TESS* eclipsing-binary population, because the catalog is shaped by spectroscopic follow-up selection and publication bias toward systems with interesting or well-constrained solutions.

5.3. Main-Sequence Comparison with the Eker et al. [8] Relations

The complete catalog is deliberately heterogeneous: it includes SB1 and SB2 systems as well as detached, semi-detached, and contact configurations. It is therefore inappropriate to calibrate single-star relations from all catalog entries. We instead use the relations of Eker et al. [8] as an external consistency test for the subset of components compatible with the main sequence. This comparison assesses the internal consistency and physical plausibility of the literature compilation; it is not a new fit to, or replacement for, the Eker et al. relations.

Eker et al. [8] selected 509 main-sequence stars in detached SB2 systems with precise absolute parameters and found that a six-piece classical power-law form provides an adequate empirical description of the mass–luminosity relation. Following their selection approach, we use the PARSEC evolutionary-model loci adopted by Eker et al. to define a conservative main-sequence envelope bounded by ZAMS and TAMS at $Z = 0.008$ and $Z = 0.040$ for detached SB2 systems. The mass–radius plane was used for this classification because masses and radii are the most directly constrained quantities in joint light-curve and radial-velocity solutions.

The resulting comparison sample contains 345 components located within the adopted main-sequence band, including 62 stars in common with Eker et al. [8] (Table S2 in the Supplementary Materials). Figure 5 shows the retained and rejected components in the mass–radius plane. Components outside the adopted envelope are retained in the parent catalog but excluded from this comparison.

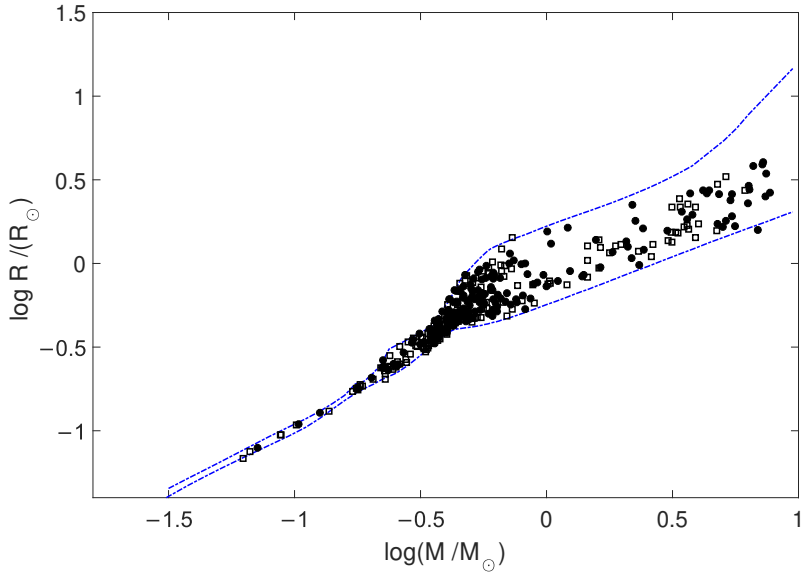

Figure 5. *Cont.*

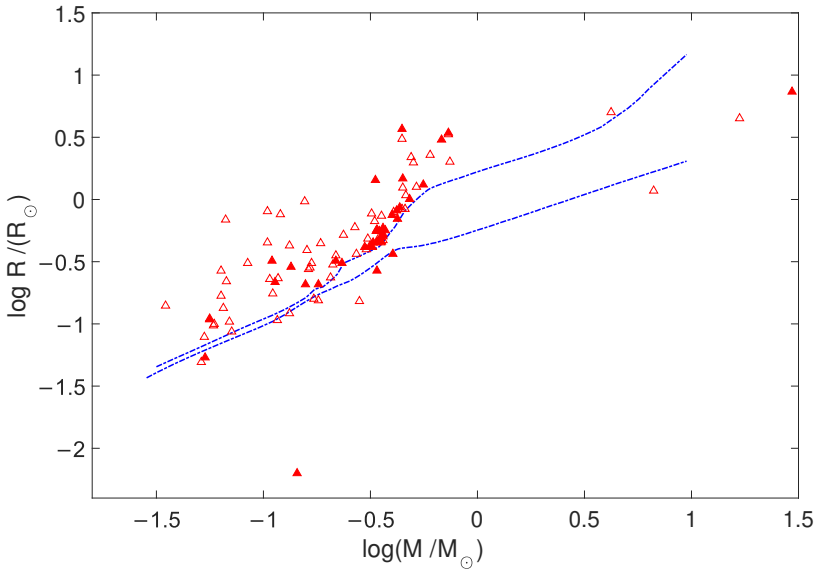

Figure 5. Mass–radius diagram used to define the main-sequence comparison sample. (**Upper panel**): components selected as main-sequence stars; filled and open markers denote primary and secondary components, respectively. (**Lower panel**): components classified as non-main-sequence stars and excluded from the comparison sample; triangles mark components classified as non-main-sequence. The dashed curves show the ZAMS ($Z = 0.008$) and TAMS ($Z = 0.040$) boundaries adopted from PARSEC models [22].

Figure 6 compares the selected main-sequence components with the interrelated mass–luminosity, mass–radius, and mass–effective-temperature relations of Eker et al. [8]. The compiled TESS sample follows the expected mass-dependent trends over the mass range covered by the catalog. This agreement provides a qualitative check that the compiled parameters preserve the expected correlations among mass, luminosity, radius, and effective temperature for ordinary main-sequence stars. The scatter around the empirical curves is consistent with the heterogeneous nature of the source literature, including differences in temperature scales, light-curve and radial-velocity modeling assumptions, metallicity, evolutionary state, and reported uncertainties. We therefore interpret Figure 6 as an external consistency check of the catalog rather than as a recalibration of the Eker et al. relations.

To quantify the comparison, we computed residuals between the catalog values and the predictions of the Eker et al. MLR, MRR, and MTR functions at the corresponding mass for each of the 345 main-sequence components. The mean residuals are $\Delta \log L = +0.0237 \pm 0.2074$ dex, $\Delta \log R = +0.0052 \pm 0.0852$ dex, and $\Delta \log T_{\rm eff} = +0.0033 \pm 0.0489$ dex. These residuals are consistent with zero within the scatter expected for heterogeneous literature parameters and support the internal consistency of the compiled catalog.

5.4. The Radius Inflation in Detached Low-Mass Binaries

Radius inflation, defined as the systematic infaltion of observed radii over stellar-evolution predictions, has been widely reported in low-mass detached eclipsing binaries (DEBs) (e.g.,Cruz et al. [23]). To examine this effect in our sample, we select systems containing two main-sequence components, at least one of which has $M < 0.8\,M_{\odot}$, from the 345 main-sequence comparison sample defined in Section 5.3, adopting the mass criterion of Feiden & Chaboyer [24]; this selection yields 34 components in total. Our adopted threshold is slightly less restrictive than the $M \leq 0.7\,M_{\odot}$ criterion used by Cruz et al. [23]. Only components satisfying this mass limit are included in the mass–radius diagram (Figure 7).

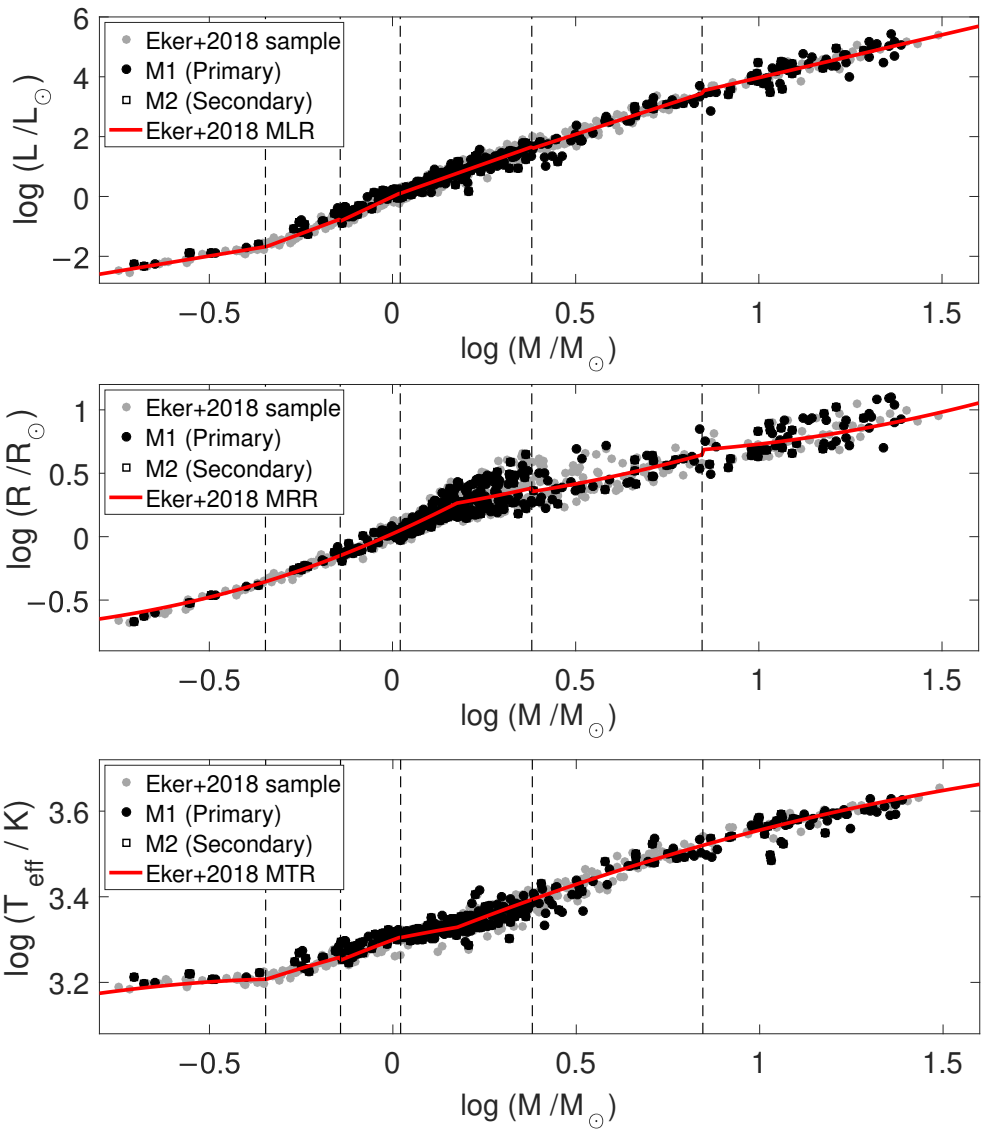

Figure 6. Comparison of the main-sequence components in this work with the interrelated mass–luminosity, mass–radius, and mass–effective-temperature relations of Eker et al. [8]. Filled circles and open squares denote primary and secondary components, respectively. The solid curves are the Eker et al. empirical relations; they are shown as an external reference and are not refitted here. Vertical lines mark the mass-domain boundaries adopted by Eker et al. [8].

Our sample also shows a tendency toward radius inflation. Despite individual measurement uncertainties, the observed radii tend to exceed stellar-evolution predictions at the corresponding masses. Figure 7 shows the standard isochrones of the Baraffe–Homeier–Allard–Chabrier 2015 (BHAC15) models for 1, 5, and 8 Gyr, indicated by solid, dot–dashed, and dashed curves, respectively. We adopt the 5 Gyr BHAC15 grid ($[M/H] = 0$, $Y = 0.28$, $L_{\rm mix} = 1.6\,H_P$) to compute the radius inflation. The theoretical radius is linearly interpolated at the catalog mass of each component, and the fractional radius inflation is defined as

$$\delta_{R,i} = \frac{R_{{\rm obs},i} - R_{{\rm model},i}}{R_{{\rm model},i}}. \tag{11}$$

Here, $R_{{\rm obs},i}$ and $R_{{\rm model},i}$ are the observed and interpolated theoretical radii, respectively. The unweighted mean over all 34 components, including negative residuals, gives a mean radius inflation of $\overline{\delta_R} = 8.4\%$ from the BHAC15 model. This definition and averaging method follow Cruz et al. [23].

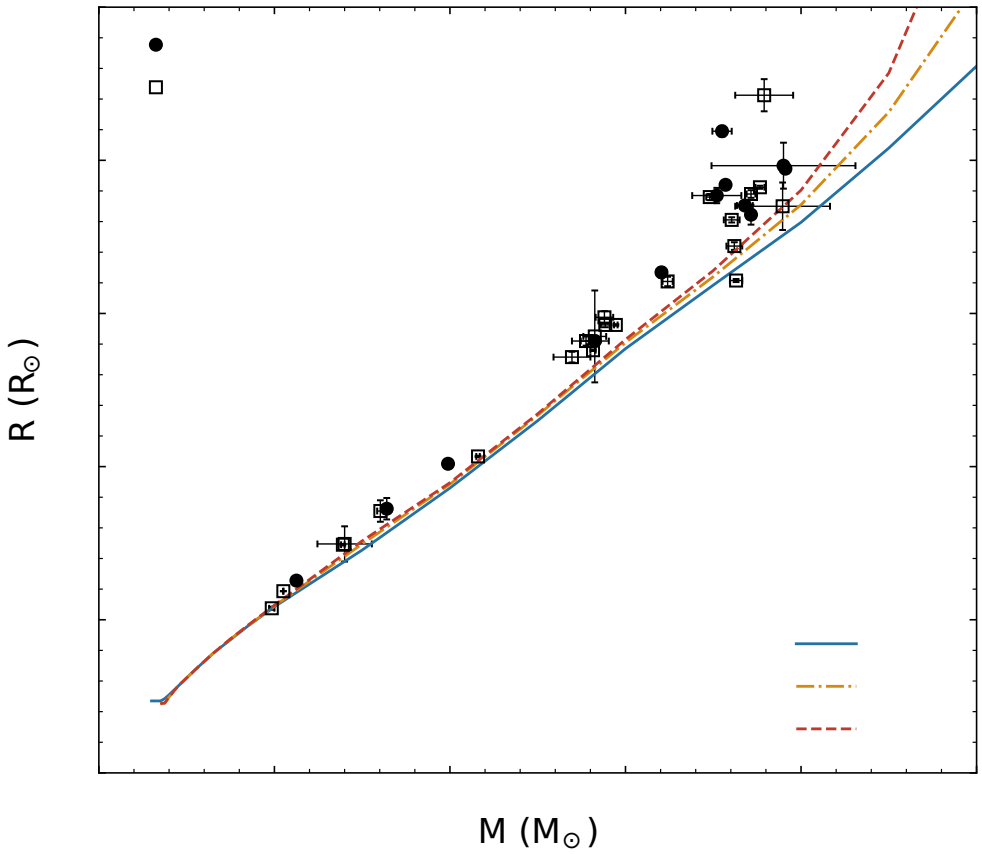

Figure 7. Mass–radius diagram for the selected low-mass main-sequence sample. Baraffe et al. [25] standard stellar models for 1, 5, and 8 Gyr are represented by solid, dot–dashed, and dashed lines, respectively. Error bars indicate the reported mass and radius uncertainties.

Cruz et al. [23] reported an overall radius inflation of approximately 20% for Kepler DEBs. Although their mass–radius diagram includes the 1, 5, and 8 Gyr BHAC15 isochrones [25], their quoted inflation value was calculated using the 5 Gyr predictions of the BCAH98 models [26]. For direct comparison, we also calculate radius inflation with the BCAH98 models and perform a robustness test using three solar-metallicity, 5 Gyr BCAH98 grids, labeled BCAH98$_{\rm iso.1}$, BCAH98$_{\rm iso.2}$ and BCAH98$_{\rm iso.3}$. Of these, BCAH98$_{\rm iso.1}$ ($[M/H] = 0$, $Y = 0.275$, $L_{\rm mix} = 1.0\,H_P$) and BCAH98$_{\rm iso.3}$ ($[M/H] = 0$, $Y = 0.282$, $L_{\rm mix} = 1.9\,H_P$) apply to all 34 components and yield mean radius inflation percentages of 5.6% and 7.6%, respectively. BCAH98$_{\rm iso.2}$ ($[M/H] = 0$, $Y = 0.275$, $L_{\rm mix} = 1.5\,H_P$) has a lower mass limit of $0.6\,M_\odot$ and covers only 17 components in our sample, giving a mean radius inflation of 8.8%. These fixed-age calculations yield offsets arising from the choice of evolutionary model parameters, rather than age estimates for individual stars. Our radius inflation rates are lower than those reported by Cruz et al. [23].

As noted by Torres & Ribas [27], Torres [28], radius discrepancies depend strongly on the adopted evolutionary models, ages and metallicities. This is one reason for the difference in inflation rates between our work and Cruz et al. [23]. Differences in main-sequence selection also contribute to this discrepancy. We identify main-sequence components using boundaries from the PARSEC evolutionary models, while Cruz et al. [23] adopt photometric luminosity classification based on a ten-color grid and clustering techniques. Our stricter selection in the mass–radius plane may remove components with large radius inflation and weaken the detected inflation signal. By contrast, Carmo et al. [29] found no significant radius inflation among DEBs selected from the Catalina Sky Survey. These diverse results

imply that modeling choices, sample properties, selection effects and analysis methods can all affect the outcome.

The present catalog enlarges the sample of low-mass main-sequence components in TESS-observed detached eclipsing binaries and provides data for future radius-inflation studies. A detailed investigation of the physical origin of this inflation (e.g., magnetic activity, rotation, spot coverage) is beyond the scope of this catalog but deserves further study using this expanded sample.

5.5. Double-Lined Spectroscopic Detectability at Low Mass Ratio

The catalog provides an empirical view of how SB2 classifications become less common toward low literature-defined mass ratios. Among the 11 systems with $q < 0.1$, only one is classified as SB2, and it is a contact binary. In the range $0.1 < q < 0.2$, the catalog contains 26 systems, of which 10 are SB2s, and 7 are detached. Thus, very low-q systems in the present compilation are predominantly classified as SB1, while the SB2 fraction increases in the $0.1 < q < 0.2$ interval.

This trend is qualitatively expected from spectroscopic detectability. At low mass ratios, the secondary component is often much fainter than the primary, and its spectral lines may be weak, blended, or hidden by rotational broadening and limited signal-to-noise ratios. Detectability also depends on the luminosity ratio, effective-temperature contrast, spectral resolution, wavelength coverage, phase sampling, and quality of the radial-velocity data. Because the catalog preserves the component conventions of the adopted literature, the quoted q values should be interpreted consistently with the definitions used in the source papers.

We therefore interpret the apparent decline in SB2 classifications below $q \sim 0.1$ as an observational trend in the present literature sample, rather than as a universal physical threshold. A quantitative SB2 detectability boundary would require homogeneous spectra, well-defined selection criteria, and injection–recovery tests, which are beyond the scope of this compilation.

6. Summary and Conclusions

We have presented a compiled literature catalog of 280 *TESS*-observed eclipsing binaries with published spectroscopic constraints, compiled from 121 peer-reviewed studies through December 2025. The catalog records identifiers, orbital and stellar parameters, uncertainties, references, provenance information, and quality flags.

The sample includes 228 SB2 and 52 SB1 systems and by morphology 249 detached, 19 semi-detached, and 12 contact binaries. It is dominated by short-period, low-eccentricity systems, with most binaries having $P_{\rm orb} < 10$ days and $e < 0.1$. This reflects both tidal circularization and observational selection and should be interpreted as a property of the current spectroscopically characterized TESS literature sample rather than the intrinsic population. By combining our catalog with theEker et al. [3] sample, we analyzed the period–eccentricity distribution by separating the systems into Hot–Hot, Hot–Cold and Cold–Cold groups. Fitting the functional form of Zanazzi [21] confirms the previously established dependence of tidal circularization on stellar type: convective systems exhibit circularization at longer periods (Hot–Cold: $P_{\rm circ} = 6.2 \pm 0.6$ d; Cold–Cold: $P_{\rm circ} = 7.4 \pm 1.3$ d) than radiative systems ($P_{\rm circ} = 3.5 \pm 0.8$ d). We also constrained empirical upper envelopes, yielding $P_{\rm env} = 3.2 \pm 0.9$ d (Hot–Cold), 6.3 ± 0.8 d (Cold–Cold), and 1.1 ± 0.2 d (Hot–Hot).

The catalog supports reproducible construction of subsamples: detached SB2 systems with well-reported uncertainties are best suited for stellar-model comparisons, while semi-detached and contact systems remain valuable for studies of binary interaction. SB1 companion parameters should be treated as inferred or model-dependent. A filtered main-sequence

sample of 345 components follows the Eker et al. [8] mass–luminosity, mass–radius, and mass–effective-temperature relations within the scatter expected from heterogeneous literature parameters, providing an external consistency check on uniform compilation. We also find a mild radius inflation for low-mass components ($M < 0.8\,M_{\odot}$) relative to standard stellar-evolution models, with a mean fractional radius inflation of $\overline{\delta_R} = 8.4\%$ (BHAC15). Alternative BCAH98 grids yield values ranging from 5.6% to 8.8%. Across the model grids examined in this work, our derived inflation rates remain weaker than the $\sim 20\%$ inflation reported for Kepler detached eclipsing binaries by Cruz et al. [23].

Overall, this machine-readable, provenance-aware catalog is designed to support target selection, detached-SB2 benchmark construction, and follow-up studies of stellar parameters and binary interaction.

Supplementary Materials: The following supporting information can be downloaded at https://www.mdpi.com/article/10.3390/universe12110358/s1, Table S1: Complete catalog of TESS eclipsing binaries with spectroscopic constraints (CSV file); Table S2: Main-sequence comparison sample of 345 components (CSV file).

Author Contributions: Conceptualization, Y.L., X.W., Y.Z., and G.L.; methodology, Y.L. and X.W.; validation, X.W.; formal analysis, X.W. and Y.L.; data curation, X.W. and Y.L.; writing—original draft preparation, X.W. and Y.L.; writing—review and editing, all authors; supervision, Y.L., Y.Z., and G.L. All authors have read and agreed to the published version of the manuscript.

Funding: This research is funded by the National Natural Science Foundation of China, grant numbers 12373111, 12533010, and 12273076; the B-type Strategic Priority Program of the Chinese Academy of Sciences, grant number XDB0560000; and the Specialized Research Fund for State Key Laboratory of Solar Activity and Space Weather.

Data Availability Statement: The complete catalog associated with this work is publicly available at https://zenodo.org/records/23944330 (accessed on 15 November 2026) (doi: 10.5281/zenodo.23944330).

Conflicts of Interest: The authors declare no conflicts of interest.

References

1. Andersen, J. Accurate masses and radii of normal stars. *Astron. Astrophys. Rev.* **1991**, *3*, 91–126. [CrossRef]
2. Torres, G.; Andersen, J.; Giménez, A. Accurate masses and radii of normal stars: Modern results and applications. *Astron. Astrophys. Rev.* **2010**, *18*, 67–126. [CrossRef]
3. Eker, Z.; Bilir, S.; Soydugan, F.; Yaz Gökçe, E.; Soydugan, E.; Tüysüz, M.; Şenyüz, T.; Demircan, O. The Catalogue of Stellar Parameters from the Detached Double-Lined Eclipsing Binaries in the Milky Way. *Publ. Astron. Soc. Aust.* **2014**, *31*, e024. [CrossRef]
4. Southworth, J. DEBCat: A Catalog of Detached Eclipsing Binary Stars. In Proceedings of the Living Together: Planets, Host Stars and Binaries, Litomyšl, Czech Republic, 8–12 September 2014.
5. Ricker, G.R.; Winn, J.N.; Vanderspek, R.; Latham, D.W.; Bakos, G.A.; Bean, J.L.; Berta-Thompson, Z.K.; Brown, T.M.; Buchhave, L.; Butler, N.R.; et al. Transiting Exoplanet Survey Satellite (TESS). *J. Astron. Telesc. Instrum. Syst.* **2015**, *1*, 014003. [CrossRef]
6. Xiong, J.; Liu, C.; Li, J.; Li, J.; Zhang, B.; Chen, X.; Luo, C.; Cao, Z.; Zhao, Y. The Eclipsing Binaries from the LAMOST Medium-resolution Survey. III. A High-precision Empirical Stellar Mass Library. *Astron. J.* **2023**, *165*, 30. [CrossRef]
7. Rowan, D.M.; Stanek, K.Z.; Kochanek, C.S.; Thompson, T.A.; Jayasinghe, T.; Blaum, J.; Fulton, B.J.; Ilyyin, I.; Isaacson, H.; LeBaron, N.; et al. Precise and Accurate Mass and Radius Measurements of Fifteen Galactic Red Giants in Detached Eclipsing Binaries. *Open J. Astrophys.* **2025**, *8*, 18. [CrossRef]
8. Eker, Z.; Bakıs, V.; Bilir, S.; Soydugan, F.; Steer, I.; Soydugan, E.; Bakis, H.; Alicavus, F.; Aslan, G.; Alpsoy, M. Interrelated main-sequence mass-luminosity, mass-radius, and mass-effective temperature relations. *Mon. Not. R. Astron. Soc.* **2018**, *479*, 5491–5511. [CrossRef]
9. Wilson, R.E.; Devinney, E.J. Realization of Accurate Close-Binary Light Curves: Application to MR Cygni. *Astrophys. J.* **1971**, *166*, 605. [CrossRef]
10. Wilson, R.E. Eccentric orbit generalization and simultaneous solution of binary star light and velocity curves. *Astrophys. J.* **1979**, *234*, 1054–1066. [CrossRef] [PubMed]
11. Prša, A.; Zwitter, T. A Computational Guide to Physics of Eclipsing Binaries. I. Demonstrations and Perspectives. *Astrophys. J.* **2005**, *628*, 426–438. [CrossRef]

12. Prša, A.; Conroy, K.E.; Horvat, M.; Pablo, H.; Kochoska, A.; Bloemen, S.; Giammarco, J.; Hambleton, K.M.; Degroote, P. Physics of Eclipsing Binaries. II. Toward the Increased Model Fidelity. *Astrophys. J.* **2016**, *227*, 29. [CrossRef]
13. Southworth, J.; Maxted, P.F.L.; Smalley, B. Eclipsing binaries in open clusters—II. V453 Cyg in NGC 6871. *Mon. Not. R. Astron. Soc.* **2004**, *351*, 1277. [CrossRef]
14. Southworth, J. Homogeneous studies of transiting extrasolar planets—I. Light-curve analyses. *Mon. Not. R. Astron. Soc.* **2008**, *386*, 1644. [CrossRef]
15. Maxted, P.F.L. ellc: A fast, flexible light curve model for detached eclipsing binary stars and transiting exoplanets. *Astron. Astrophys.* **2016**, *591*, A111. [CrossRef]
16. Copperwheat, C.M.; Marsh, T.R.; Dhillon, V.S.; Littlefair, S.P.; Hickman, R.; Gansicke, B.T.; Southworth, J. Physical properties of IP Pegasi: An eclipsing dwarf nova with an unusually cool white dwarf. *Mon. Not. R. Astron. Soc.* **2010**, *402*, 1824. [CrossRef]
17. Irwin, J.M.; Quinn, S.N.; Berta, Z.K.; Latham, D.W.; Torres, G.; Burke, C.J.; Charbonneau, D.; Dittmann, J.; Esquerdo, G.A.; Stefanik, R.P.; et al. LSPM J1112+7626: Detection of a 41 Day M-dwarf Eclipsing Binary from the MEarth Transit Survey. *Astrophys. J.* **2011**, *742*, 123. [CrossRef]
18. Corcoran, K.A.; Barlow, B.N.; Schaffenroth, V.; Heber, U.; Wasler, S.; Irgang, A. Eclipsing Binaries Found by the EREBOS Project: Gaia DR2 6097540197980557440-a Deeply Eclipsing sdB+dM System. *Astrophys. J.* **2021**, *918*, 28. [CrossRef]
19. Van Eylen, V.; Winn, J.N.; Albrecht, S. Orbital Circularization of Hot and Cool Kepler Eclipsing Binaries. *Astrophys. J.* **2016**, *824*, 15. [CrossRef]
20. Justesen, A.B.; Albrecht, S. Temperature and Distance Dependence of Tidal Circularization in Close Binaries: A Catalog of Eclipsing Binaries in the Southern Hemisphere Observed by the TESS Satellite. *Astrophys. J.* **2021**, *912*, 123. [CrossRef]
21. Zanazzi, J.J. A Tale of Two Circularization Periods. *Astrophys. J.* **2022**, *929*, L27. [CrossRef]
22. Bressan, A.; Marigo, P.; Girardi, L.; Salasnich, B.; Dal Cero, C.; Rubele, S.; Nanni, A. PARSEC: Stellar tracks and isochrones with the PAdova and TRieste Stellar Evolution Code. *Mon. Not. R. Astron. Soc.* **2012**, *1*, 127–145. [CrossRef]
23. Cruz, P.; Aguilar, J.F.; Garrido, H.E.; Diaz, M.P.; Solano, E. Detached eclipsing binaries from the Kepler field: Radii and photometric masses of components in short-period systems. *Mon. Not. R. Astron. Soc.* **2022**, *515*, 1416–1429. [CrossRef]
24. Feiden, G.A.; Chaboyer, B. Reevaluating the Mass-Radius Relation for Low-mass, Main-sequence Stars. *Astrophys. J.* **2012**, *757*, 42. [CrossRef]
25. Baraffe, I.; Homeier, D.; Allard, F.; Chabrier, G. New evolutionary models for pre-main sequence and main sequence low-mass stars down to the hydrogen-burning limit. *Astron. Astrophys.* **2015**, *577*, A42. [CrossRef]
26. Baraffe, I.; Chabrier, G.; Allard, F.; Hauschildt, P.H. Evolutionary models for solar metallicity low-mass stars: Mass-magnitude relationships and color-magnitude diagrams. *Astron. Astrophys.* **1998**, *337*, 403–412.
27. Torres, G.; Ribas, I. Absolute dimensions of the M-type eclipsing binary YY Geminorum (Castor C): A challenge to evolutionary models in the lower main-sequence. *Astrophys. J.* **2002**, *567*, 1140–1165. [CrossRef] [PubMed]
28. Torres, G. Fundamental properties of lower main-sequence stars. *Astron. Nachr.* **2013**, *334*, 4–9. [CrossRef]
29. Carmo, A.; Ferreira Lopes, C.E.; Papageorgiou, A.; Jablonski, F.J.; Rodrigues, C.V.; Drake, A.J.; Cross, N.J.G.; Catelan, M. Recovering variable stars in large surveys: EA_{up} Algol-type class in the Catalina Survey. *Mon. Not. R. Astron. Soc.* **2020**, *498*, 2833–2844. [CrossRef]

Disclaimer/Publisher's Note: The statements, opinions and data contained in all publications are solely those of the individual author(s) and contributor(s) and not of MDPI and/or the editor(s). MDPI and/or the editor(s) disclaim responsibility for any injury to people or property resulting from any ideas, methods, instructions or products referred to in the content.